Contents lists available at ScienceDirect

Applied Clay Science

Research Paper

Mineralogical and geochemical characterization of Johnson's baby powder from 1985: Evidence of contamination

Hannah Wudke [a], Kenneth Brown [b], Madeline Murchland [a], Morgan Gillis [a], Kailee Gokey [a], Justin Bank [a], Marion Lytle [a], Claire L. McLeod [a], Mark P.S. Krekeler [a,c,*]

[a] Department of Geology and Environmental Earth Science, Miami University, 250 South Patterson Avenue, Oxford, OH 45056, United States of America
[b] Department of Geology and Environmental Geoscience, DePauw University, 2 E. Hanna Street, Greencastle, IN 46135, United States of America
[c] Department of Mathematical & Physical Sciences, Miami University—Hamilton, Hamilton, OH 45011, United States of America

ARTICLE INFO

ABSTRACT

A single bottle of unopened Johnson's baby powder with a manufacturing date of 1985 was investigated for potential geochemical contaminants of concern. Study of 3 replicate samples via basic powder X-ray diffraction (XRD) indicates talc is the dominant phase present with chlorite ± serpentine and no other major impurities are observed. Scanning electron microscopy (SEM) documented the presence of Ni as a minor component in observed Fe-sulfides and Cr was detected in chromite and/or chromian magnetite. Transmission electron microscopy (TEM) documented the presence of Ni within individual platy and fibrous talc particles. Repeat analysis ($n = 10$) of pressed powders ($n = 5$) via handheld X-ray fluorescence (XRF) yielded SiO_2 contents of 57.40 to 58.28 wt% and MgO contents of 29.90 to 30.79 wt%. Data also documents the presence of Cr, Ni, Cu, Zn. Cu and Zn are interpreted to occur in Fe-sulfides. Subsequent duplicate analysis ($n = 2$) of 3 talc samples via high resolution inductively coupled plasma mass spectrometry (HR-ICP-MS) detected 4 trace metals present of concern: V, Co, Cr, and Ni. Across all sample runs ($n = 6$), V averaged 10.6 ppm (± 0.5 ppm at 2σ), Co averaged 55.0 ppm (± 4.3 ppm at 2σ), Cr averaged 400.9 ppm (± 11.4 ppm at 2σ), and Ni averaged 1395.9 ppm (± 105 ppm at 2σ). While a precise geologic source for the studied talc cannot be unequivocally identified based on the data collected in this study (and the sample bottle alone), a comparison with global talc deposits indicates a product origin likely associated with (ultra)mafic-hosted talc deposits based on Ni (ppm) and Cr (ppm) contents, as opposed to carbonate metasedimentary-hosted deposits.

From this work, it can therefore be concluded that Ni- and Cr-bearing particles made it into the baby powder production chain of this manufacturer in 1985. This study provides a foundation for future mineral and geochemical characterization of past, present, and future consumer talc-related products and may provide context for health-related studies.

1. Introduction

Talc is a hydrous phyllosilicate mineral with an ideal chemical formula of $Mg_3Si_4O_{10}(OH)_2$, having a crystalline structure with a sheet of $MgO_4(OH)_2$ octahedra between two sheets of tetrahedral SiO_4 layers resulting in a trioctahedral 2:1 layer (e.g., Gatta et al., 2013). Owing to the presence of weak van der Waals forces primarily between adjacent 2:1 layers, talc is an extremely soft mineral (Mohs hardness scale = 1) and has been extensively used in a variety of industries, such as paper, ceramics, insulation, plastics, and agriculture (National Minerals Information Center, 2022). Talc commonly is, or was, used in many personal care products, including baby powder. The geological nature of talc deposits is usually such that talc mined for personal care products is dominantly sourced from either altered ultramafic and mafic-hosted deposits, or carbonate metasedimentary-hosted deposits (e.g., Chidester, 1962; Chidester et al., 1964; Greene, 1995; Van Gosen et al., 2004; Materials Research L3C, 2020).

The association of asbestiform minerals in talc-based products and materials is well recognized (e.g., Lüchtrath and Schmidt, 1959; Cralley et al., 1968; Rohl et al., 1976; Blount, 1991; Van Gosen et al., 1998;
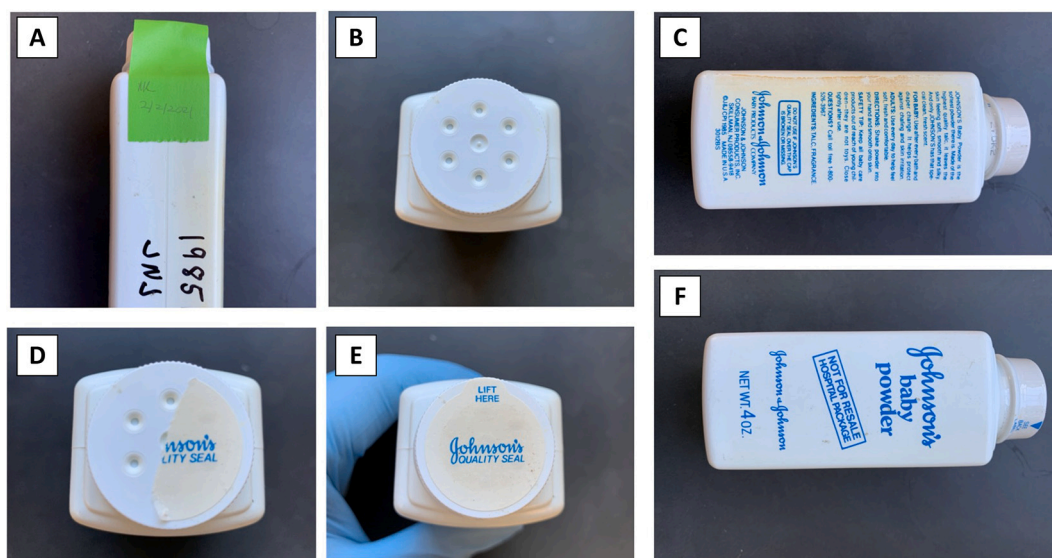

Fig. 1. Images of the 1985 Johnson's baby powder sample showing various states. A.) The sample is taped closed for future investigations. B.) Shows the clean opening of the bottle, D. shows partial opening of the bottle and E. show the unopened state. C.) and F.) also show the bottle in an unopened state with plastic seal on top and the front and back of the bottle. The 1985 date is visible in panel C.

IRSST, 2012; Millette, 2015; IWGACP, 2021). It has also been established that significant gaps in the approaches to characterizing and documenting talc materials for potential asbestos have occurred (Rosner et al., 2019; Tran et al., 2019; Bird et al., 2021; IWGACP, 2021). Accordingly, questions exist regarding the presence of other contaminants that are of environmental or human health concern in talc-based products (and their potential) sources such as metal contamination. The nature, form, and extent of potential metal contaminants in talc-based consumer products is a major consumer product safety question that has received little attention compared to well-documented asbestos issues (e.g., Cralley et al., 1968; Blount, 1991; Van Gosen et al., 1998; IWGACP, 2021).

Baby powder has been under scrutiny for asbestos contamination for over half a century (e.g., Lüchtrath and Schmidt, 1959; Cralley et al., 1968; Rohl, 1974; Rohl et al., 1976; Girion, 2018; NBC News, 2019; Loftus, 2020; IWGACP, 2021). However, one aspect of talc-based personal care talc products (such as baby powder) that has not been investigated extensively is the potential occurrence of metals with links to human health concerns and/or the presence of other non-talc minerals. Due to the protolith of some talc deposits being ultramafic or mafic igneous rocks (e.g., Chidester et al., 1964; Greene, 1995; Nkoumbou et al., 2008), several metals of concern such as nickel (Ni) and chromium (Cr) have the potential to occur within talc-based consumer products. Historical samples of talc-based baby powder are limited. For this study, a single bottle of unopened Johnson's baby powder (Fig. 1) with a product date of 1985 was acquired from Conard Metcalf (Simmons Hanley Conroy firm) and a comprehensive geochemical and mineralogical investigation conducted. This sample was specifically selected owing to its age and the time period that it represents: a time thought to be when the manufacturer produced talc product using talc ore from Vermont. However, it is stated here that it is not possible to unequivocally identify the precise provenance of this talc, and/or the associated talc mine.

In this work we present the first detailed study that aims to constrain the deposit type which sourced a talc-based product. This study demonstrates the feasibility and effective use of integrating multiple analytical methods from electron microscopy for particle characterization, to bulk chemical composition (e.g., XRF, HR-ICP-MS).

2. Materials and methods

Sample material from the 1985 Johnson's baby powder bottle was characterized for its bulk mineralogical and elemental composition by powder X-ray diffraction (XRD) using a Bruker D8 Advance X-ray diffractometer in the Department of Geology and Environmental Earth Science at Miami University, by scanning electron microscopy (SEM) and energy dispersive spectroscopy (EDS) using a Zeiss Supra 35 VP field emission scanning electron microscope (FESEM) at Miami University's Center for Advanced Microscopy and Imaging (CAMI), by Transmission Electron Microscopy (TEM) using a JEOL JEM 2100 TEM operated at 200 kV (also housed in CAMI), by X-ray fluorescence (XRF) using a Bruker Tracer 5 g handheld XRF in the Department of Geosciences at DePauw University, Indiana, and by High Resolution Inductively Coupled Plasma Mass Spectrometry (HR-ICP-MS) using a Nu Attom ES in the Department of Geology and Environmental Earth Science at Miami University.

Basic powder XRD analysis was used to identify major mineral phases in samples with the Bruker D8 Advance X-ray diffractometer using Cu Kα radiation. Three samples were analyzed as rotating pack mounts from 4° to 70° 2Θ, with a step size of 0.01° 2Θ at 3 s/step. This basic method was used to simply confirm the presence or absence of major phases (e.g., talc, magnesite) and not as a screening for the occurrence of minor or trace mineral(s) (including asbestos). Regarding crystallographic notation with respect to the use of Miller indices, by convention the triclinic systematic would require the longest axis to be defined as the c-axis. Some researchers follow this convention and thus designate the stacking direction as being along [0k0] (Gatta et al., 2013). For traditions followed specifically in the clay mineral and phyllosilicate literature, the stacking of 2:1 layers is in the [00l] direction and the b-axis (or [0k0]) functionally contains the most crystallographic complexity as details of the stacking direction are most evident (Bailey, 1988). For these reasons we elect to follow Bailey convention in labeling basic XRD data and discussion of TEM data.

For sample investigation via SEM-EDS, sample powder was mounted onto an aluminum stub of 10 mm diameter with a carbon adhesive tab. Sample analysis was undertaken using variable pressure with nitrogen (N2) as the compensating gas. The FESEM is equipped with a backscatter detector (BSD) and an EDS detector (Bruker Quantax). Both the sample preparation technique and the instrument have been routinely incorporated into a variety of recent mineralogical studies (e.g., Krekeler

Table 1

Summary of bulk XRF analyses on 5 baby powder samples (average of 10 repeat analyses reported).

	Sample JNJA (n=10)	2σ	Sample JNJB (n=10)	2σ	Sample JNJC (n=10)	2σ	Sample JNJD (n=10)	2σ	Sample JNJE (n=10)	2σ
MgO wt.%	30.09	0.81	29.90	0.61	29.96	0.53	30.18	0.83	30.79	1.28
SiO$_2$ wt.%	57.87	0.37	57.40	0.44	57.95	0.63	58.28	0.52	58.23	0.21
Cl wt.%	0.25	0.01	0.20	0.03	0.21	0.02	0.25	0.01	0.27	0.02
CaO wt.%	0.14	0.01	0.15	0.01	0.14	0.01	0.14	0.01	0.13	0.00
MnO wt.%	0.01	0.00	0.01	0.003	0.01	0.003	0.01	0.002	0.01	0.003
Fe$_2$O$_3$ wt.%	3.44	0.02	3.38	0.02	3.45	0.02	3.45	0.03	3.42	0.02
Cr ppm	533	43	539	48	541	58	542	33	518	45
Ni ppm	2093	31	2149	37	2066	50	2078	20	2049	41
Cu ppm	67	3	69	3	68	5	67	4	66	5
Zn ppm	39	3	40	7	40	4	39	2	39	3
Sr ppm	2	1	2	1	2	1	2	1	3	1
MgO/SiO$_2$	0.52		0.52		0.52		0.52		0.53	

et al., 2010; LeGalley and Krekeler, 2013; Dietrich et al., 2019; Velázquez Santana et al., 2020; Oglesbee et al., 2020; Lindeman et al., 2020; Klein and Krekeler, 2020; Flett et al., 2021; O'Shea et al., 2021).

For transmission electron microscopy (TEM) analytical work, ~0.05 g of sample powder was suspended in approximately 2 mL of ethanol in glass vials and shaken. Resulting suspensions were allowed to settle for 30 s. Aliquots of approximately 5 μL were placed onto a 3 mm copper grid with lacey-carbon film and allowed to air dry. A JEOL JEM-2100 transmission electron microscope that was operated at 200 kV and equipped with a Bruker EDS detector was used for bright-field imaging and chemical analysis. Digital images were acquired with a Gatan Orius SC 200D CCD camera. Selected-area electron diffraction (SAED) patterns were used to characterize crystallinity and orientation. Similar approaches using this instrument have been published in previous investigations of other (geo)materials (e.g., LeGalley and Krekeler, 2013; Paul et al., 2017; Burke et al., 2017; Cymes et al., 2017, 2020, 2021; O'Shea et al., 2021).

EDS analysis on fine grained mixed mineral, or mixed phase samples with multiple chemical components as described above within the context of both SEM and TEM, requires an understanding of the limitations associated with signal contributions as well as potential peak overlap. X-ray emission lines used to identify elements provided by Bruker software include: O K = 0.525 keV; Mg K = 1.254 keV; Al K = 1.487 keV; Si K$_\alpha$ = 1.740 keV, (nominally K$_\beta$ = 1.837 keV); S K$_\alpha$ = 2.309 keV (nominally K$_\beta$ = 2.465 keV); Cr K$_\alpha$ = 5.410 keV and K$_\beta$ = 5.947 keV; Fe K$_\alpha$ = 6.399 keV and K$_\beta$ = 7.060 keV; Ni K$_\alpha$ = 7.480 keV and K$_\beta$ = 8.267 keV; Cu K$_\alpha$ = 8.036 keV and K$_\beta$ = 8.903 keV. The ubiquitous nature of oxygen in silicate and oxide phases in substrate (or adjacent particles), scatter from the copper grid, and the lacey carbon substrate, collectively contribute O, Cu, and C signal to EDS spectra. For SEM-EDS, some of the Al signal may originate from the Al-stubs. The detection limit for EDS is approximately 0.08 wt% (e.g., Kuisma-Kursula, 2020).

The Bruker Tracer 5 g handheld XRF unit is fitted with a rhodium (Rh) source, a graphen window silicon drift detector (SDD) detector, and

Table 2

Concentration (in ppm) of trace elements analyzed in 3 replicates (A,B,C) of JNJ1985. Each replicate was analyzed twice.

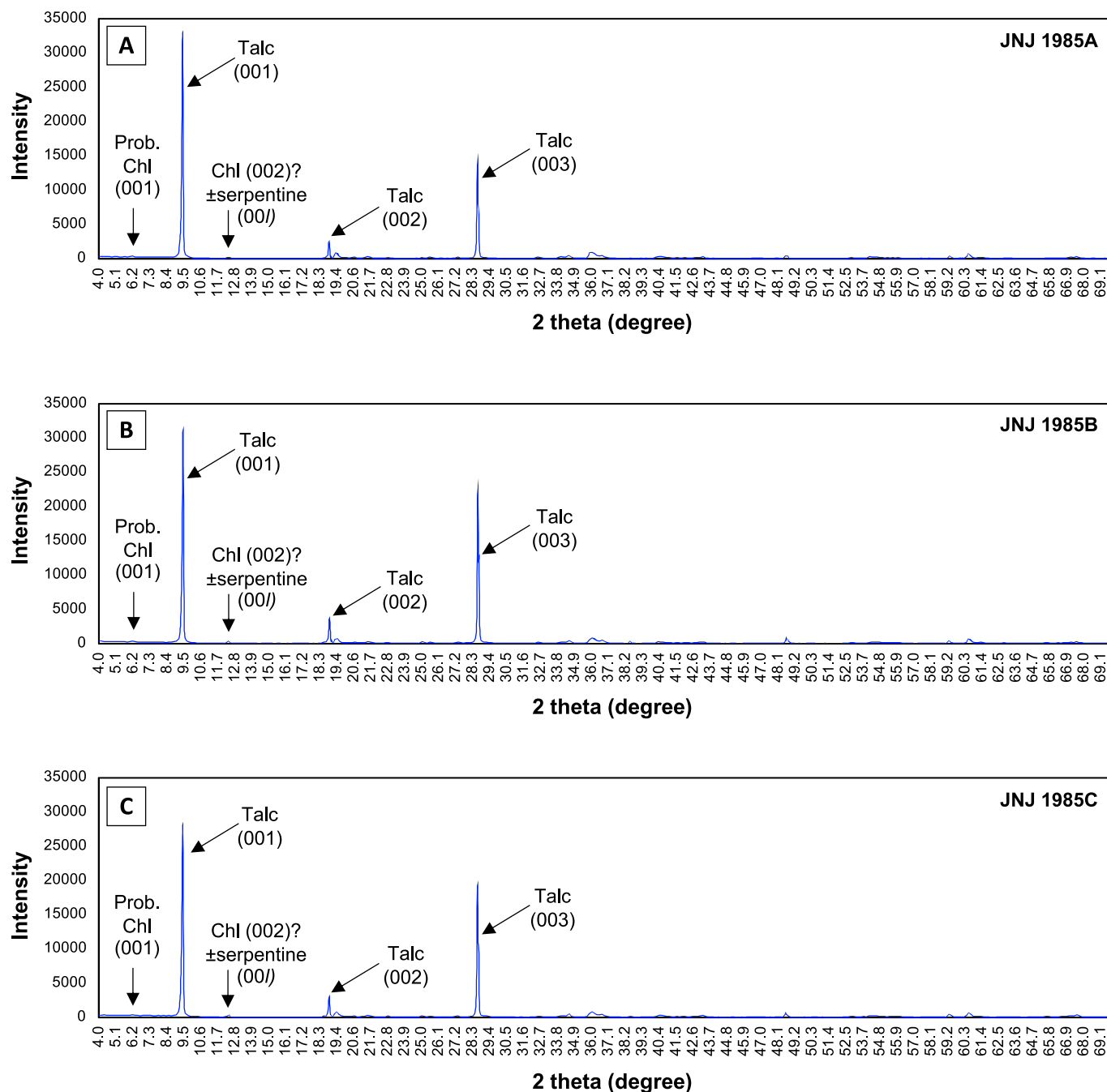|	JNJ1985H-A				JNJ1985H-B				JNJ1985H-C				JNJ1985H-A,B,C	
	run 1	run 2	average	2σ	run 1	run 2	average	2σ	run 1	run 2	average	2σ	average	2σ
Sc	1.1	1.1	1.1	0.1	1.2	1.1	1.1	0.1	1.2	1.2	1.2	0.1	1.1	0.1
V	10.8	10.7	10.7	0.0	10.8	10.2	10.5	0.9	10.5	10.4	10.5	0.1	10.6	0.5
Cr	402.9	405.8	404.3	4.1	394.1	395.4	394.7	1.8	408.2	399.0	403.6	13.1	400.9	11.4
Co	53.1	52.3	52.7	1.0	56.5	54.5	55.5	2.9	58.0	55.8	56.9	3.0	55.0	4.3
Ni	1367.4	1320.6	1344.0	66.1	1415.1	1377.1	1396.1	53.7	1472.5	1422.5	1447.5	70.8	1395.9	105.0
Cu	bd	bd	-	-	bd	bd	-	-	1.4	1.3	1.3	0.2	1.3	0.2
Zn	21.5	21.6	21.5	0.1	26.4	24.9	25.6	2.0	24.6	23.5	24.1	1.5	23.7	3.9
Ga	0.4	0.4	0.4	0.0	0.4	0.4	0.4	0.0	0.4	0.4	0.4	0.1	0.4	0.0
Rb	0.0	0.1	0.1	0.0	0.1	0.1	0.1	0.0	0.1	0.1	0.1	0.0	0.1	0.0
Sr	1.2	1.2	1.2	0.0	1.1	1.1	1.1	0.1	1.2	1.1	1.2	0.1	1.1	0.1
Y	0.0	0.0	0.0	0.0	0.0	0.0	0.0	0.0	0.0	0.0	0.0	0.0	0.0	0.0
Zr	0.2	0.2	0.2	0.0	0.2	0.2	0.2	0.0	0.4	0.3	0.3	0.1	0.2	0.2
Nb	0.0	0.0	0.0	0.0	0.0	0.0	0.0	0.0	0.0	0.0	0.0	0.0	0.0	0.0
Cs	0.0	0.0	0.0	0.0	0.0	0.0	0.0	0.0	0.0	0.0	0.0	0.0	0.0	0.0
Ba	0.1	0.0	0.0	0.1	0.1	0.1	0.1	0.0	0.1	0.1	0.1	0.0	0.1	0.1
La	0.0	0.0	0.0	0.0	0.0	0.0	0.0	0.0	0.0	0.0	0.0	0.0	0.0	0.0
Ce	0.0	0.0	0.0	0.0	0.0	0.0	0.0	0.0	0.0	0.0	0.0	0.0	0.0	0.0
Pr	0.0	0.0	0.0	0.0	0.0	0.0	0.0	0.0	0.0	0.0	0.0	0.0	0.0	0.0
Nd	0.0	0.0	0.0	0.0	0.0	0.0	0.0	0.0	0.0	0.0	0.0	0.0	0.0	0.0
Sm	0.0	0.0	0.0	0.0	0.0	0.0	0.0	0.0	0.0	0.0	0.0	0.0	0.0	0.0
Eu	0.0	0.0	0.0	0.0	0.0	0.0	0.0	0.0	0.0	0.0	0.0	0.0	0.0	0.0
Gd	0.0	0.0	0.0	0.0	0.0	0.0	0.0	0.0	0.0	0.0	0.0	0.0	0.0	0.0
Tb	0.0	0.0	0.0	0.0	0.0	0.0	0.0	0.0	0.0	0.0	0.0	0.0	0.0	0.0
Dy	0.0	0.0	0.0	0.0	0.0	0.0	0.0	0.0	0.0	0.0	0.0	0.0	0.0	0.0
Ho	0.0	0.0	0.0	0.0	0.0	0.0	0.0	0.0	0.0	0.0	0.0	0.0	0.0	0.0
Er	0.0	0.0	0.0	0.0	0.0	0.0	0.0	0.0	0.0	0.0	0.0	0.0	0.0	0.0
Tm	0.0	0.0	0.0	0.0	0.0	0.0	0.0	0.0	0.0	0.0	0.0	0.0	0.0	0.0
Yb	0.0	0.0	0.0	0.0	0.0	0.0	0.0	0.0	0.0	0.0	0.0	0.0	0.0	0.0
Lu	0.0	0.0	0.0	0.0	0.0	0.0	0.0	0.0	0.0	0.0	0.0	0.0	0.0	0.0
Hf	0.0	0.0	0.0	0.0	0.0	0.0	0.0	0.0	0.0	0.0	0.0	0.0	0.0	0.0
Ta	0.0	0.0	0.0	0.0	0.0	0.0	0.0	0.0	0.0	0.0	0.0	0.0	0.0	0.0
Pb	1.2	1.2	1.2	0.1	1.2	1.2	1.2	0.0	1.2	1.2	1.2	0.1	1.2	0.1
Th	0.0	0.0	0.0	0.0	0.0	0.0	0.0	0.0	0.0	0.0	0.0	0.1	0.0	0.0
U	0.0	0.0	0.0	0.0	0.0	0.0	0.0	0.0	0.0	0.0	0.0	0.0	0.0	0.0

Fig. 2. A-C Basic powder X-ray diffraction patterns for samples A, B, and C. Major reflections are labelled using the conventional phyllosilicate designations. Probable or possible major peaks for chlorite ± serpentine are also labelled.

an 8 mm collimator. Staged in a laboratory configuration, bulk samples were analyzed under atmospheric conditions for 90 s using a Fundamental Parameters (FP) three phrase GeoExploration calibration (30 s at 30 kV; 30 s at 50 kV; 30 s at 15 kV). The data is presented in Table 1. Accuracy and precision of the analytical session was monitored by analyzing 14 replicates of reference talc sample BCS-RM No. 203a (British Ceramic Research Ltd. and Bureau of Analyzed Samples Ltd, 2018). Unknown samples (baby powder) and BCS-RM No. 203a were prepared by placing approximately 4–5 g of material into a Chemplex XRF sample container and analyzed through a 4.0 μm thick Prolene thin-film (Laperche and Lemière, 2021). Unknowns ($n = 5$) were analyzed in replicates of 10. The FP GeoExploration calibration has the following limits of detection, as reported by the manufacturer: SiO_2 (0.001 wt%), TiO_2 (0.004 wt%), Al_2O_3 (0.14 wt%), Fe_2O_3 (0.003 wt%), MnO (0.001

wt%), MgO (0.5 wt%), CaO (0.003 wt%), K_2O (0.006 wt%), P_2O_5 (0.004 wt%), and Cl (0.01 wt%). The limit of detection for Ni and Cu is 5 ppm, Zn and Cr is 10 ppm, and Sr is 1 ppm. These trace elements are specifically noted here as they represent those that were detected during sample analysis (see later). It is however also noted here that while major element data for talc reference material BCS-RM No. 203a are available (see Table 1), trace element data are not. Within this context, the XRF was utilized as a screening tool to evaluate the potential presence of trace metals of concern.

Trace elements (Sc, V, Cr, Co, Ni, Cu, Zn, Ga, Rb, Sr, Y, Zr, Nb, Cs, Ba, La, Ce, Pr, Nd, Sm, Eu, Gd, Tb, Dy, Ho, Er, Tm, Yb, Lu, Hf, Ta, Pb, Th, U) were subsequently determined by solution High Resolution Inductively Coupled Plasma Mass Spectrometry (HR-ICP-MS; Table 2 using a Nu Instruments Attom ES in the Department of Geology and Environmental
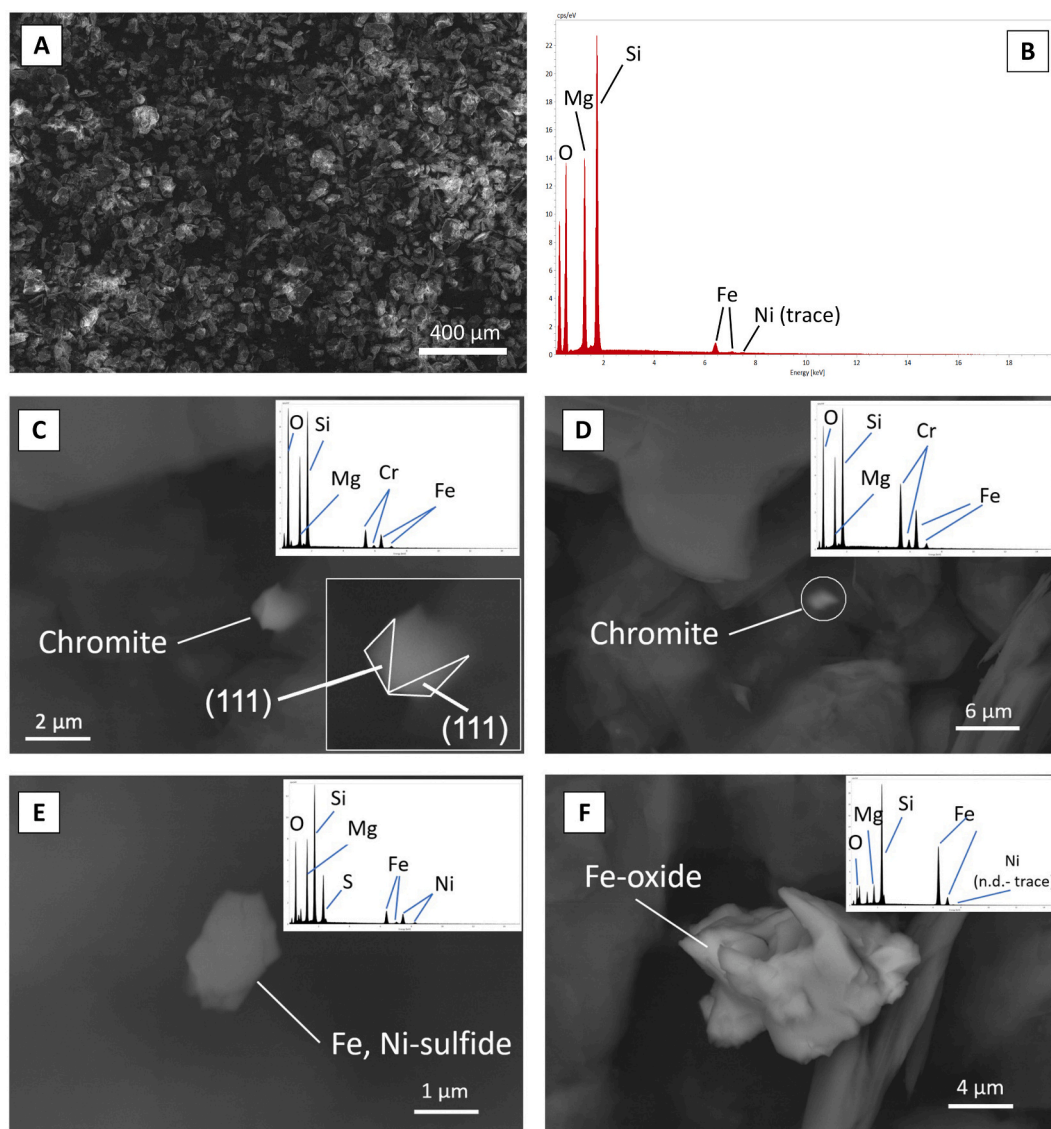
Fig. 3. SEM images in BSD with paired EDS spectra showing mineralogical impurities in talc. Panel A shows a low magnification image which captures the general texture and particle size of sample material with B being an EDS spectra taken over the field of view. Si, Mg, and O dominate the spectrum with minor Fe and trace amounts of Ni also present. Panels C and D show examples of Fe-Cr oxide, interpreted as chromite. C shows a single crystal of chromite with an inset panel where (111) faces are identified. Panel E shows an image of a Fe-sulfide with minor nickel contents. Panel F shows a Fe-oxide with trace Ni content. Mg and Si are interpreted to originate from the talc substrate.

Earth Science at Miami University. ~0.05 g of the unknown baby powder sample was dissolved in triplicate ($n = 3$; samples A, B, and C, see Table 2) using HNO_3 and HF digestion following the methods of Kelley et al. (2003) and Anderson et al. (2021). Raw HR-ICP-MS data were corrected for instrumental drift using an internal drift correction of 1 ppb In in the NuQuant data analysis program. Five standards (BHVO-2, DNC-1, GSP-2, SCo-1, SGR-1) were used to produce calibration curves that were linear to $R > 0.999$. A standard (BCR-2) was run as an unknown throughout the run. Samples were analyzed in duplicate, with each run consisting of 5 individual sweeps of data and an overall reproducibility of $\leq 2\%$ RSD. A summary of standard data acquired during this work (reported as an average) is presented in Supplementary Table 1 alongside accepted values for each element, for each standard. Collectively this dataset is summarized in Supplementary Fig. 1.

3. Results

3.1. Powder X-ray diffraction

Basic powder XRD patterns for sample materials show talc as the dominant phase (e.g., JCPDS 29–1493) with lesser amounts of chlorite $\pm$ serpentine (see Fig. 2). Using Bailey conventions, talc has pronounced (001), (002) and (003) reflections. Chlorite has minor (001) reflections, and the chlorite (002), or potentially serpentine (00*l*) or combined overlapping chlorite (002) or serpentine (00 l) were slightly more intense than the chlorite (001). All chlorite and potential serpentine reflections were far less intense than talc diffraction peaks. No major peaks of other phases were reliably identified. This is consistent with powder XRD having a detection limit of a few weight percent (Bish and Post, 1989) as well as the observations of phases be electron microscopy (see below).
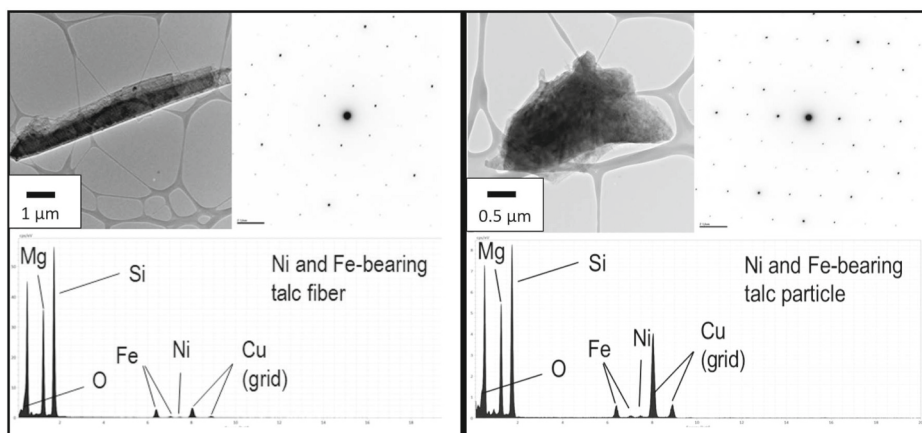
Fig. 4. Examples of Ni-bearing talc particles. Left data set shows talc fiber having a > 3:1 aspect ratio having an electron diffraction pattern indicative of high crystallinity (along [hk0] conforming to Bailey convention) with appreciable Fe and minor Ni present. Cu is derived from the grid. Right data set shows an example of talc particle approximately 3 μm in diameter with an electron diffraction pattern indicative of high crystallinity (along [hk0] conforming to Bailey stacking convention for phyllosilicates) with appreciable Fe and minor Ni present. Accompanying EDS spectral range for both particles shown from 0 to 20 keV.

3.2. Scanning electron microscopy (SEM)

SEM data indicate that non-talc minerals occur in the product (Fig. 3). Equant subhedral individual crystals of an Fe-Cr-rich oxide are observed. These crystals are approximately 1 to 2 μm in diameter and examples occur showing them as distinct from talc particles in addition to being inclusions in talc particles. Based on the occurrence of (111) faces observed, and their Fe-Cr chemistry, these minerals are interpreted either as chromite or chromian magnetite (Fig. 3C, D). Chromite or chromian magnetite particles are present in trace amounts and estimated to constitute <0.1% of the volume of sample examined in BSD. This is based on visual estimations. Fe-sulfide minerals are also observed, and these minerals have minor to trace amounts of Ni (Fig. 3E). Fe-sulfide particles are subhedral in texture and are approximately 3 to 25 μm in diameter. Fe-sulfide particles are also present in trace amounts and estimated to constitute <0.2% of the volume of sample examined in BSD. This is based on visual estimations. Fe-oxides with trace amounts of Ni are also observed (Fig. 3F) although not commonly.

3.3. Transmission electron microscopy (TEM)

TEM data for studied talc particles are presented in Fig. 4. Talc particles exhibit two morphologies. Platy morphology talc constitutes ~99% of the population (right panel, Fig. 4) and fibrous talc constitutes ~1% of the population (left panel, Fig. 4). In TEM samples, platy particles are commonly 3 to 7 μm in diameter whereas fibrous particles are commonly >4 μm in length and have aspect ratios >3:1. SAED for both particle types yield single, or near single, crystal patterns of high quality with well-formed discrete spots for [hk0] (see Fig. 4). Spot EDS spectra on talc particles show Mg, Si, and O, minor amounts of Fe (approximately 0.5 to 2.0 wt% Fe_2O_3), and minor NiO concentrations of approximately 0.1 to 0.2 wt% (see Fig. 4). Distinct EDS peaks in spot analysis for Ni are small and/or near detection limits.

3.4. X-ray fluorescence (XRF)

Averages of ten replicate XRF analyses on five subsamples of talc from the studied talc product bottle are provided in Table 1, alongside reported reference material values for the major oxides (see Section 2 earlier). Select major oxides and trace elements are summarized in Fig. 5. The abundance of SiO_2 (57.40 to 58.28 wt%) and MgO (29.90 to 30.79 wt%), in addition to MgO/SiO_2 ratios (0.52 and 0.53), varied minimally and are consistent with the product being dominated by talc

based on mineral stoichiometry. Cr concentrations averaged 535 ppm (±58 ppm, 2σ) and varied from 518 to 542 ppm; Ni concentrations averaged 2087 ppm (±50 ppm, 2σ) and varied from 2049 to 2149 ppm; Cu concentrations varied minimally from 66 to 69 ppm; Zn concentration varied minimally from 39 to 40 ppm; and Sr concentrations are 2 to 3 ppm.

3.5. High resolution inductively coupled plasma mass spectrometry (HR-ICP-MS)

Element abundances from each analytical run (1 and 2) of each subsample (A, B, C) are presented in Table 2 alongside their respective 2σ values. Average abundances for each element (and the 2σ) are also reported in the last two columns of Table 2 ($n = 6$). The majority of trace elements analyzed for were below detection limit (e.g., the rare earth elements: La to Lu). The only elements detected at >10 ppm were (in order of increasing concentration) V, Co, Cr, and Ni. Across all 6 sample runs, V averaged 10.6 ppm (±0.5 at 2σ), Co averaged 55.0 ppm (±4.3 at 2σ), Cr averaged 400.9 (±11.4 at 2σ), and Ni averaged 1395.9 ppm (±105 at 2σ). This data is summarized in Fig. 6 alongside the averages for each subsample (A, B, C) and the associated 2σ.

4. Discussion

Powder XRD was conducted solely for the purpose of confirming major phase relationships and established that the sample material was dominantly talc and chlorite ± serpentine. Major issues exist with powder X-ray diffraction study of talc and baby powder, particularly in the context of studies of asbestos (e.g., Rosner et al., 2019). Powder XRD was not executed in this study as a means to screen for asbestos, although the possibility of chrysotile exists as indicated by the ~7 Å peaks observed. XRD data indicates there was no unusual or unexpected mineral (e.g., large amounts of olivine, pyroxene, carbonate, chromate minerals) or metal, alloy, or unexpected chemical (Ni or Cr, steel, or synthetic chemical) in the baby powder. XRD data supports the argument that Ni and Cr is in large part from talc particles, with contribution of minor phases observed in electron microscopy data. The baby powder does not appear to be aberrantly manufactured, having unusual or uncommon minerals or production metals from equipment accidentally incorporated, or synthetic chemicals accidentally incorporated.

Bulk chemical analysis of talc-based baby powder via XRF and HR-ICP-MS are interpreted to reflect the mixture of talc, Fe-sulfides, and chromite or chromian magnetite. This is consistent with observations via SEM and TEM (see Figs. 3 and 4). The occurrence of Ni and Cr is
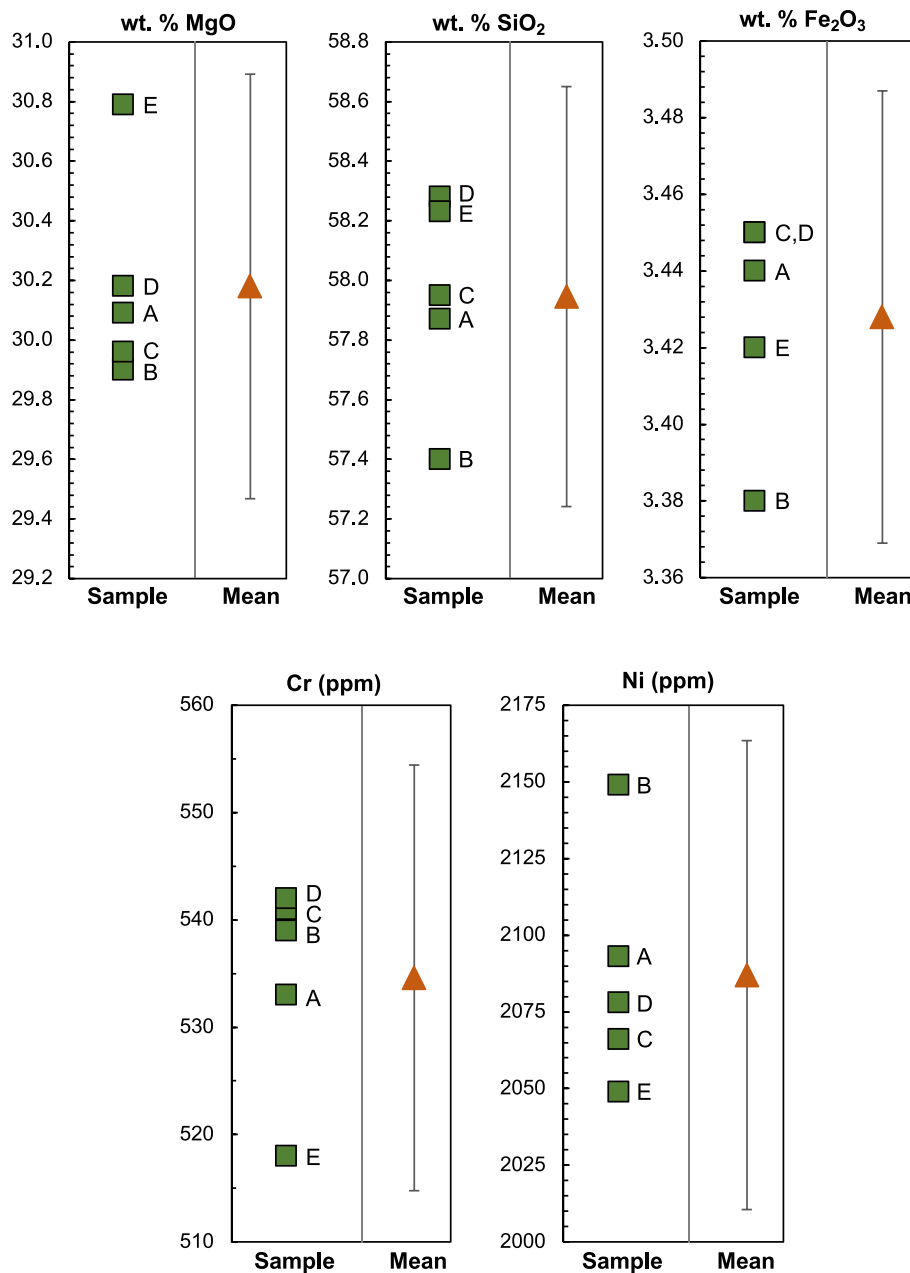
Fig. 5. Results of replicate handheld XRF analyses (A-E). The average composition of each oxide or element for samples A-E are summarized alongside the associated 2 standard deviation for that analyte.

primarily interpreted to be inherent to the products' geologic source (i. e., its protolith). Specifically, Ni is interpreted to be inherent in the talc and in the Fe-sulfides while Cr is inherent to the chromite or chromian magnetite. In the discussion that follows below, the trace element data collected via HR-ICP-MS in this study is considered. The trace element data acquired via handheld XRF is not considered any further.

While a precise geologic source cannot be identified based on the data collected during this study and the bottle alone, it is known that Johnson & Johnson obtained talc from Vermont (Girion, 2018; Landen, 2018; Vermont Business Magazine, 2018). From Van Gosen et al. (2004), Vermont talc deposits are associated with ultramafic rocks (as opposed to carbonate-hosted deposits) and are described as being "typical of 'black wall' deposits". Briefly, these "black wall" deposits are associated with regional metamorphic and related metasomatic processes which result in the generation of zoned "alteration rinds" and the development of; talc-carbonate zones, high purity talc zones, Ca-amphibole-chlorite

zones, and a transitional zone near the protolith (Van Gosen et al., 2004).

While a direct source for the consumer talc in this study cannot unequivocally be identified, the bulk geochemical signatures of talc associated with (ultra)mafic- and carbonate-hosted deposits can establish a broad geological framework. Table 3 summarizes the concentrations of V, Cr, Co, and Ni in talc deposits from across the globe, in both (ultra)mafic- and carbonate-hosted settings. The (ultra)mafic deposits summarized include the talc schists from the Boumnyebel area of Cameroon (Nkoumbou et al., 2008), talc from the Rod Umm El-Farag region in Egypt (El-Sharkawy, 2000), talc from the Oaxaca and Puebla ore deposits in Mexico (Pi-Puig et al., 2020), talc-carbonate ore from the Altermark talc province in Norway (Karlsen et al., 2000), talcose rocks from the Gilów deposit in Poland (Gil et al., 2022), and talc samples from the Emirdağ talc deposit in Turkey (Ersoy et al., 2013). The carbonate-hosted deposits summarized include talc ore from the
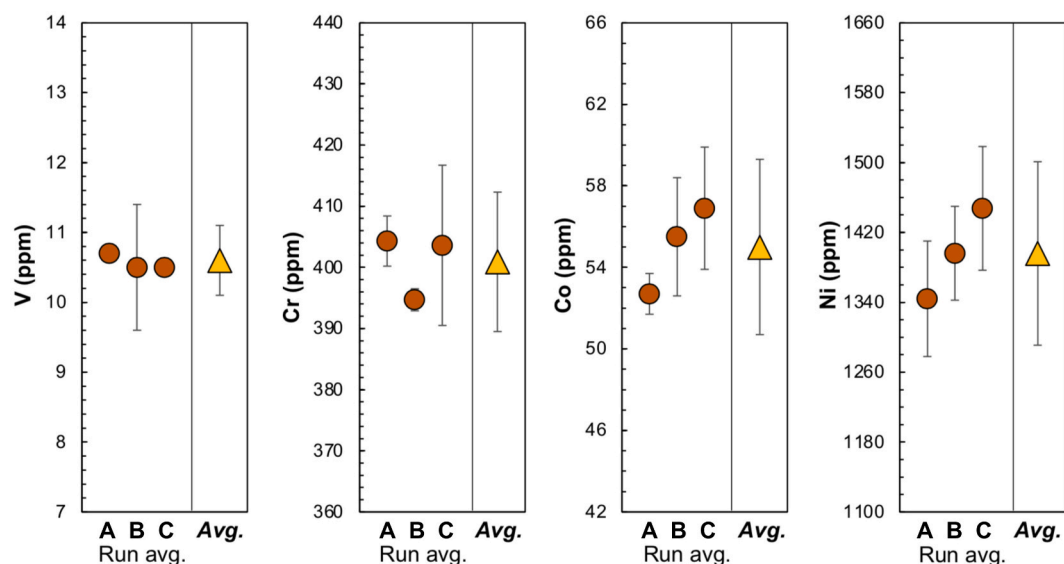
Fig. 6. Results of replicate ICP-MS analyses (samples A-C). The average composition (run average) for V, Cr, Co, and Ni in each sample is shown in the orange-filled circle alongside the 2SD. When no error bars are visible, they are smaller than the symbol size. The average from all 3 samples (6 runs total) is shown to the right in each panel in the yellow-filled triangle. Data is summarized in Table 2. (For interpretation of the references to colour in this figure legend, the reader is referred to the web version of this article.)

Table 3

Compilation of V, Cr, Co, and Ni concentrations in ultramafic and carbonate hosted talc deposits. All values in ppm.

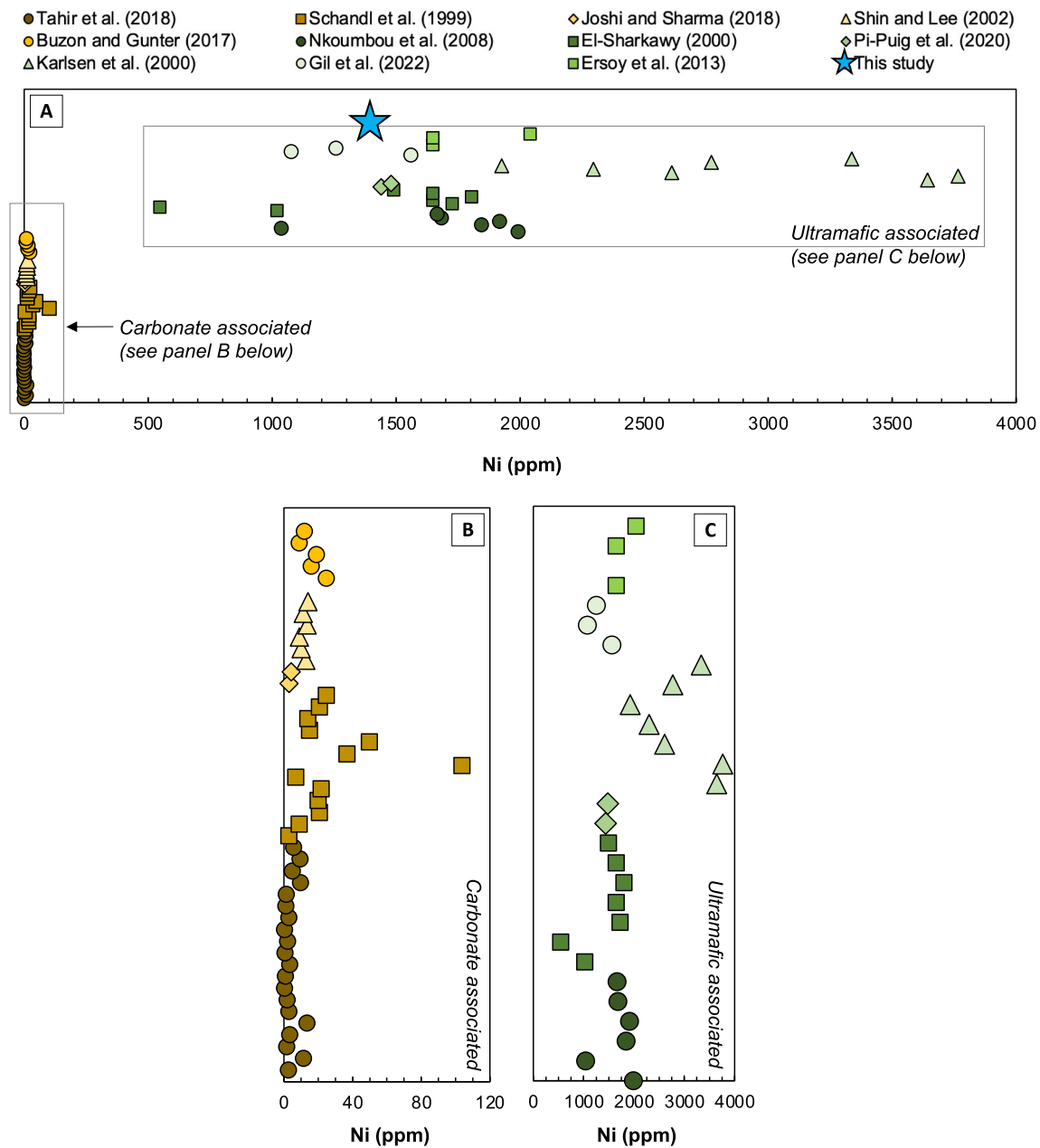| ULTRAMAFIC	V	Cr	Co	Ni	CARBONATE	V	Cr	Co	Ni
Cameroon	-	3606	89.2	1994	**Afghanistan**	6.3	9.3	1.2	2.8
Nkoumbou et al. (2008)	13.3	1722	51.2	1040	*Tahir et al. (2018)*	2.9	10.5	7.1	11.5
	10.3	1296	72.7	1846		5.4	22.8	2.2	1.9
	31.1	2392	93.2	1919		7.9	15.1	2.5	3.6
	22.1	1900	72.9	1685		3.7	7.4	11.9	13.6
	19.7	2075	68.9	1668		-	9.4	10.4	3.1
Egypt	2.0	616	43.0	1022		4.6	12.5	0.8	2.1
El-Sharkawy (2010)	5.0	4858	37.0	550		-	15	1.4	0.5
	15.0	1916	51.0	1729		0.6	8.3	0.2	1.1
	6.0	1505	52.0	1650		24.0	13.4	2.9	3.6
	7.0	2053	56.0	1807		9.0	9.3	1.5	0.7
	9.0	1163	54.0	1650		3.1	9.9	4.5	2.2
	8.0	1163	54.0	1493		0.9	11.5	1.2	0.6
Mexico	37.0	1360	40.0	1440		2.4	14.1	1.0	3.1
Pi-Puig et al. (2020)	26.0	2280	46.0	1480		3.5	10.1	1.0	1.2
Norway	40.0	1735	63.0	3644		3.1	10.5	0.1	1.5
Karlsen et al. (2000)	58.0	3634	74.0	3766		5.2	12.1	2.4	9.8
	33.0	1860	55.0	2612		1.7	11.4	1.5	5.0
	35.0	2085	51.0	2297		3.3	17.3	1.5	9.7
	22.0	1054	41.0	1927		0.0	14.9	2.0	5.8
	24.0	1450	62.0	2771	**Egypt**	-	3.0	1.0	3.0
	31.0	1733	52.0	3337	*Schandl et al. (1999)*	-	3.0	1.0	9.0
Poland	-	821	82.5	1650		-	2.0	1.0	21.0
Gil et al. (2022)	-	1368	82.8	-		-	4.0	1.0	20.0
	-	1916	83.6	1650		-	3.0	1.0	22.0
	-	2395	84.0	2043		-	4.0	2.0	7.0
						-	41.0	46.0	104.0
						-	63.0	29.0	37.0
						-	7.0	2.0	50.0
						-	3.0	3.0	15.0
						-	8.0	2.0	14.0
						-	25.0	6.0	21.0
						-	4.0	2.0	25.0
						-	27.0	36.7	-
						-	61.0	41.1	-
						-	14.0	34.6	-
						-	44.0	17.6	-
					India	97.3	2.5	1.0	3.1
					Joshi and Sharma (2014)	114.2	6.0	1.3	4.4
					South Korea	-	11.6	5.8	12.8
					Shin and Lee (2002)	-	15.7	4.6	10.2
						-	12.8	5.1	9.0
					USA	11.0	18.0	-	25.0
					Buzon and Gunter (2017)	4.0	2.0	-	16.0
						3.0	10.0	-	19.0
						4.0	4.0	-	9.0
						5.0	10.0	-	12.0

Fig. 7. A. Summary of Ni (ppm) contents from a global population of talc deposits associated with carbonate and (ultra)mafic geologic environments. B. Summary of Ni (ppm) contents in carbonate-hosted talc deposits. C. Summary of Ni (ppm) contents in (ultra)mafic-hosted talc deposits.

Nangarhar Province in Afghanistan (Tahir et al., 2018), talc ore bodies from the Atshan Talc deposit in Egypt (Schandl et al., 1999), talc from the Lesser Himalaya, Kumaun, India (Joshi and Sharma, 2015), talc ore from the Hwanggangri Mineralized Zone in South Korea (Shin and Lee, 2002), and "commercial grade" talc from the southwest Montana talc deposits in the USA (Buzon and Gunter, 2017). As shown (see Table 3), the abundances of Ni and Cr are distinct between these two types of deposits with abundances often two orders of magnitude greater in (ultra)mafic-related deposits. The data summarized in Table 3 is presented in Figs. 7 and 8 alongside the average abundance of Ni and Cr (in ppm) in the studied Johnson & Johnson 1985 talc product. As shown in Fig. 7A, Ni contents in talc are typically <100 ppm for carbonate-hosted deposits and often <40 ppm. For carbonate-associated talc hosted in ultramafic deposits, Ni contents are typically >1000 ppm and show more variability (e.g., Altermark talc, Norway, which ranges from 1927 ppm to 3766 ppm; Karlsen et al., 2000). In Fig. 7B and C, the deposit

types are shown individually. The maximum variation in Ni concentration at a single location for a carbonate-hosted deposit is 101 ppm (3 ppm to 104 ppm from the Atshan Talc deposit in Egypt; Schandl et al., 1999). For ultramafic deposits, Cr contents are typically >500 ppm (often up to ~2000 ppm) and show more variability than Cr in carbonate-related deposits (see Fig. 8A). In Fig. 8B and C, the locations are shown individually with the maximum variation of Cr at a single location for a ultramafic deposit 2310 ppm (1296 ppm to 3606 ppm from the Boumnyebel area of Cameroon; Nkoumbou et al., 2008). Also shown in Figs. 7A and 8A is the average concentration of Ni and Cr respectively from the 1985 Johnson & Johnson talc consumer product of this study. As shown, the average Ni (ppm) concentration of 1395.9 is geochemically akin to that of ultramafic-hosted talc deposits and distinct from that expected from carbonate-hosted talc deposits. For Cr, the average concentration in the 1985 Johnson & Johnson talc of 400.9 ppm is the most akin to the Cr abundances associated with several of the
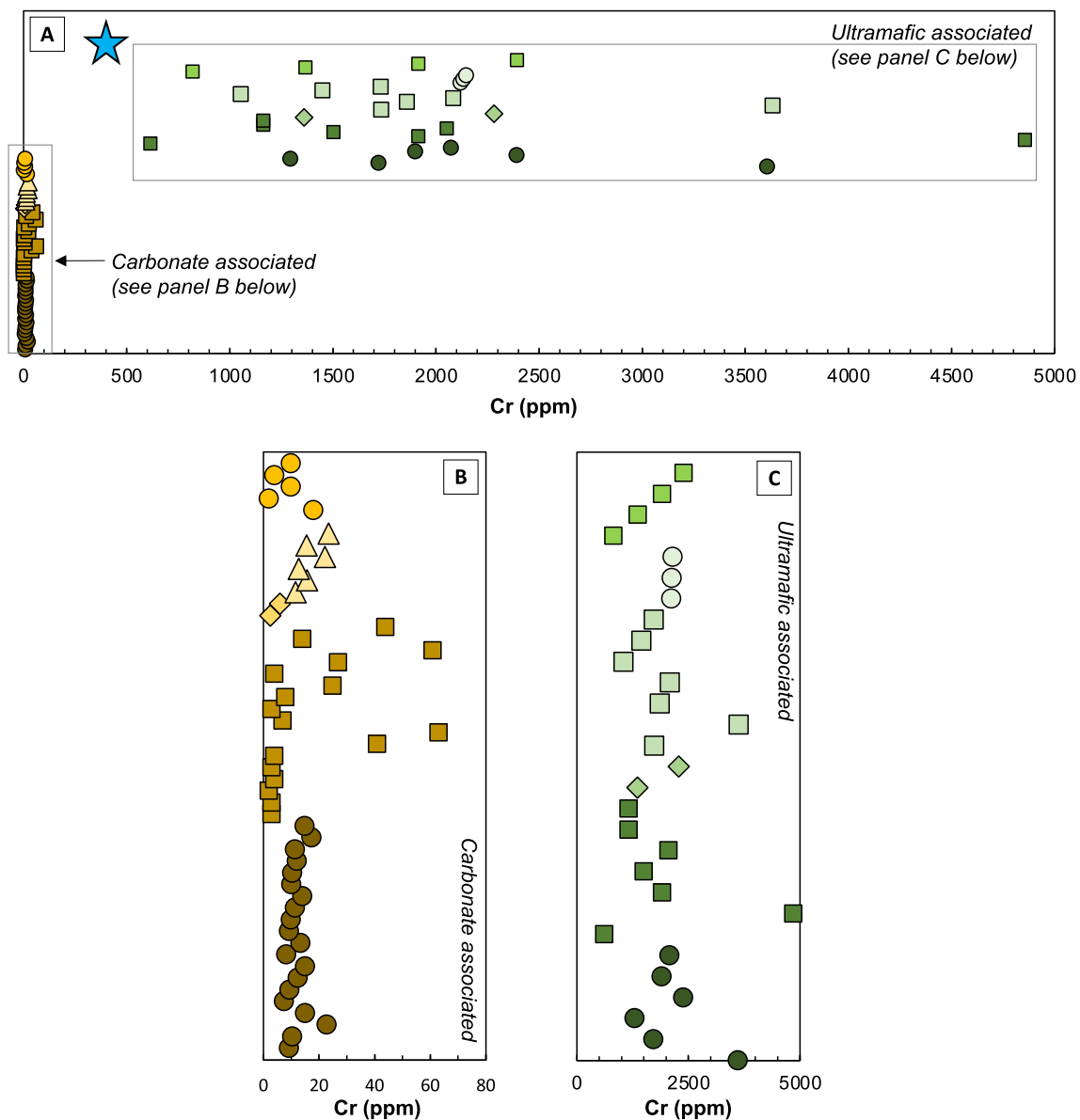
Fig. 8. A. Summary of Cr (ppm) contents from a global population of talc deposits associated with carbonate and (ultra)mafic geologic environments. Literature source data cited in Fig. 7. B. Summary of Cr (ppm) contents in carbonate-hosted talc deposits. C. Summary of Cr (ppm) contents in (ultra)mafichosted talc deposits.

ultramafic-hosted talc deposits, albeit at the lower end of the range summarized. This value is however still an order of magnitude greater than the range in Cr associated with carbonate-hosted deposits (see Fig. 7). In summary, the Ni and Cr signatures of the studied 1985 Johnson & Johnson consumer talc are more consistent with an origin from an ultramafic talc source that a carbonate-hosted deposit. (See Table 4.)

It is known that Johnson & Johnson obtained talc from Vermont although there is limited data for direct comparison. For example, Chidester (1962) investigated talc-bearing rocks in Vermont and indicated that Cr and Ni were present in talc from the region. Specifically, Chidester (1962) states "Chromium occurs in the serpentine and talc-carbonate rock chiefly in chromian magnetite, but in a few places occurs in translucent grains of chromite; both talc and serpentine also contain small amounts of Cr." Chidester (1962) interpreted chromite as a relict mineral that had persisted through both the alteration of peridotite to the serpentinite lithology, and then persisted through serpentinite to the talc-carbonate rock transition. Chidester (1962) also indicated that serpentinite, talc carbonate rock, and steatite commonly

have concentrations of NiO on the order of a tenth of a weight percent (0.1 wt%, or 786 ppm Ni). The chemical formula for talc associated with two talc-producing mines are also provided. Talc from the Waterbury mine: $(Mg_{2.86}Fe^{2+}_{0.12},Ni_{0.01}Fe^{3+}_{0.01})_{2.99}(Al_{0.01}Si_{3.99})_4O_{10}(OH)_{1.97}$ has 0.13 wt% NiO (1022 ppm Ni) while talc from the Johnson Mine: $(Mg_{2.73}Fe^{2+}_{0.23},Ni_{0.01}Fe^{3+}_{0.01})_{2.97}(Al_{0.01}Si_{3.99})_4O_{10}(OH)_{1.91}$ has 0.18 wt% NiO (1415 ppm Ni). While Ni is recognized in other talc deposits globally (see Figs. 7 and 8), based on currently available information and for the time frame in question, Vermont would be the only viable source Johnson & Johnson had access to that appears to match the chemical compositions observed in the present study. Discussion in July 2022 with Jon Kim at the Vermont Geological Survey indicates that the state survey has no historic samples from any Vermont talc mines.

Medical predictions or causes of disease associated with talc use are beyond the scope of this work however it is well established that Ni and Cr are metals which are of concern to human health. Specifically, Cr (III) is recognized as a micronutrient and is not of as significant concern while Cr (VI) is classified as a group 1 carcinogen (IARC, 2012). However, the fate and transport of Cr, and the potential oxidation in body

Table 4
Summary of talc deposit characteristics.

Ultramafic and mafic-hosted talc deposits		
Location	*Geologic context of talc data in Figs. 7 and 8*	*Reference*
Rod Umm El-Farag, Egypt	Pure talc (>90% talc) from talc lenses hosted within ultramafic rocks	El-Sharkawy (2000)
Altermark talc province, Norway	Ophiolite complex, zoned talcified ultramafic lenses, The talc carbonate zone is one of these three zones	Karlsen et al. (2008)
The Boumnyebel area, Cameroon	Talc ore deposits are composed of talc schists (and hornblendites)	Nkoumbou et al. (2008)
Emirdağ talc deposit, Turkey	Five alteration zones associated with altered gabbro including actibolite zone and a "talc-level"	Ersoy et al. (2013)
Puebla and Oaxaca complexes, Mexico	Talc ore deposits (currently non-productive) associated with serpentinite bodies	Pi-Puig et al. (2020)
Carbonate metasedimentary-hoted deposits		
Location	*Geologic context of talc data in Figs. 7 and 8*	*Reference*
Atshan talc deposit, Hamata, Egypt	Talc orebodies protoliths were "impure dolomitic limestones locally intercalated with clastic sediments"	Schandl et al. (1999)
Poongjeon talc deposit, South Korea	Metamorphic contact aureole. Talc ore bodies are surrounded by calc-silicate rocks in dolomitic marbles	Shin and Lee (2002)
Talc deposit, Deoban Fm. Lesser Himalaya, India	Talc occurs with interlayered dolomite and magnesite, varies from "schistose to compact massive in nature"	Joshi and Sharma (2014)
Commercial grade talc-rich rocks, Montana, USA	Talc exists in dolomitized marbles: "Hydrothermally altered carbonate talc deposits"	Buzon and Gunter (2016)
Talc deposit, Nangarhar Province, Afghanistan	Talc ore bodies are interlayered with carbonate host rocks; magnesite, dolomite, tremolite replaced	Tahir et al. (2018)

fluids of Cr from chromite, chromian magnetite, or talc is unclear. Cr (VI) is directly linked to several health problems including asthma, ulcers, lung inflammation, renal damage, kidney disease, cancer of the lung, and negative impacts on reproduction (e.g., IARC, 2012; Tchounwou et al., 2012; Teklay, 2016). The oxidation state of Cr and form as ionic substitution in talc, should therefore be investigated in the future, as should geochemical reactions in human fluid analogs.

IARC classified Ni as a group 2B metal and thus is a possible carcinogen (IARC, 2012b). The primary health effect of Ni in humans is an allergic reaction with 10–20% of the U.S. population being sensitive (ATSDR, 2005). Lung cancer was also found to develop in rats exposed to Ni compounds that have a low solubility in water (ATSDR, 2005). Although the 2+ oxidation state of Ni should be dominant in silicate and oxide materials, the form of Ni in talc, should be investigated in the future as should geochemical reactions in human fluid analogs.

Cu and Zn are recognized to substitute into pyrite and Abraitis et al. (2004) reports a range of concentrations for Cu in pyrite of ~1 ppm to ~7 wt% and for Zn, 10 to 10,000 ppm. Cu and Zn are commonly observed in other Fe-sulfides at concentrations of ~1 ppm to a few thousand ppm (e.g., Rottier et al., 2016; Mansur et al., 2021). The minerals controlling the concentrations of Cu and Zn in the 1985 Johnson's baby powder sample are unclear, however it is postulated here that these metals are in the Fe-sulfides observed.

Although this study is not a medical exposure study it should be noted that the particles interpreted as chromite or chromian magnetite are observed at size fractions PM_{10} to $PM_{2.5}$. If suspended in air, particles of this size have the potential to be inhaled and make it into the upper respiratory track or deep into the lungs of humans (e.g., Plumlee et al., 2006). Similarly, some of the Fe-sulfide particles observed were $< PM_{10}$ and thus if suspended in air could also be inhaled and make it into the upper respiratory track (Plumlee et al., 2006). Talc particles could also

be inhaled if they were to be suspended in air and were to subsequently enter the upper respiratory track as some are associated with the PM_{10} fraction (Plumlee et al., 2006). This study may therefore provide some mineralogical and geochemical context for future medical exposure studies.

5. Summary

This investigation has shown unequivocally that Ni and Cr made it into the baby powder production chain of this manufacturer in 1985. Repeat analysis of sample powders via XRD document the dominance of talc in the studied product (as expected). Minor reflection peaks in XRD patterns could potentially also be interpreted as representing the presence of chlorite and/or serpentine, and chrysotile is possible. Sample analysis via SEM and TEM documented the occurrence of Fe-sulfides (which are associated with Ni), and chromite and chromian magnetite both of which are associated with the presence of Cr. Bulk Ni and Cr contents determined via HR-ICP-MS from triplicate sample analysis averaged 1395.9 ppm ($\pm$105 ppm at 2σ) and 400.9 ppm ($\pm$11.4 ppm at 2σ) respectively.

While a geologic source for this talc-based consumer product cannot be unequivocally traced, the bulk trace element contents of Ni and Cr can be used to evaluate a potential origin within the content of (ultra) mafic and carbonate-hosted talc ore deposits. From comparison with a global talc dataset, the magnitude of Ni (ppm) and Cr (ppm) contents are more consistent with derivation from an (ultra)mafic-hosted talc deposit where Ni contents are typically >1000 ppm. This study therefore opens questions regarding the nature of contamination of talc-based consumer and industrial products not only from this manufacturer but potentially from other manufacturers who have used the same (or similar) talc-dominated geologic sources. Detailed mineralogical and geochemical

studies that incorporate evaluation of oxidation state should be carried out on other historical product samples as well as geologic source materials (if available). This work also provides potential mineralogical and geochemical context and justification for future medical related studies on diseases associated with talc exposure.

CRediT authorship contribution statement

Hannah Wudke: Conceptualization, Formal analysis, Investigation, Methodology, Writing – original draft, Writing – review & editing. **Kenneth Brown:** Formal analysis, Investigation, Methodology, Resources, Validation, Writing – original draft, Writing – review & editing. **Madeline Murchland:** Investigation, Methodology, Writing – original draft. **Morgan Gillis:** Formal analysis, Investigation, Methodology, Writing – original draft. **Kailee Gokey:** Investigation, Methodology, Writing – original draft. **Justin Bank:** Investigation, Methodology. **Marion Lytle:** Formal analysis, Investigation, Methodology, Writing – original draft. **Claire L. McLeod:** Formal analysis, Funding acquisition, Investigation, Methodology, Project administration, Resources, Software, Supervision, Validation, Visualization, Writing – original draft, Writing – review & editing. **Mark P.S. Krekeler:** Conceptualization, Data curation, Formal analysis, Funding acquisition, Investigation, Methodology, Project administration, Resources, Supervision, Validation, Visualization, Writing – original draft, Writing – review & editing.

Declaration of competing interest

The authors declare the following financial interests/personal relationships which may be considered as potential competing interests: I (Mark Krekeler) work as an expert witness in asbestos litigation cases in the United States specifically for the Simmons Hanly Conroy, Kazan Law, Motely Rice, Dean Omar Branham Shirley, and Levy Konigsberg firms. These firms did not provide financial support for this study to me or any authors of this study for this project.

Data availability

Data will be made available on request.

Acknowledgements

Appendix A. Supplementary data

Supplementary data to this article can be found online at https://doi.org/10.1016/j.clay.2023.107252.

References

Abraitis, P.K., Pattrick, R.A.D., Vaughan, D.J., 2004. Variations in the compositional, textural and electrical properties of natural pyrite: a review. Int. J. Miner. Process. 74, 41–59. https://doi.org/10.1016/j.minpro.2003.09.002.

Anderson, M., Wanless, V.D., Perfit, M., Conrad, E., Gregg, P., Fornari, D., Ridley, W.I., 2021. Extreme heterogeneity in mid-ocean ridge mantle revealed in lavas from the 8° 20′ N near-axis seamount chain. Geochem. Geophys. Geosyst. 22 (1) https://doi.org/10.1029/2020GC009322 e2020GC009322.

ATSDR, 2005. Toxicologic Profile for Nickel. https://www.atsdr.cdc.gov/toxprofiles/tp15.pdf.

Bailey, S.W., 1988. Hydrous phyllosilicates (exclusive of micas). Rev. Mineral. 19, 725. https://doi.org/10.1515/9781501508998.

Bird, T., Steffen, J.E., Tran, T.H., Egilman, D.S., 2021. A review of the talc industry's influence on federal regulation and scientific standards for asbestos in talc. New Solut.: J. Environ. Occup. Health Policy 0, 1–18. https://doi.org/10.1177/1048291121996645.

Bish, D.L., Post, J.E., 1989. Modern powder diffraction. Rev. Mineral. 20, 369.

Blount, A.M., 1991. Amphibole content of cosmetic and pharmaceutical talcs. Environ. Health Perspect. 94, 225–230. https://doi.org/10.1289/ehp.94-1567955.

British Ceramic Research Ltd. and Bureau of Analyzed Samples Ltd, 2018. Analysis Report for British Chemical Standard – Reference Material, BCS-RM No. 203a Talc. https://www.basrid.co.uk/images/bascertificates2013/bcs_ss-crm/BCS-RM%20203a%20Jul2018.pdf.

Burke, M., Rakovan, J., Krekeler, M.P.S., 2017. A study by electron microscopy of gold and associated minerals from Round Mountain, Nevada. Ore Geol. Rev. 91, 708–717. https://doi.org/10.1016/j.oregeorev.2017.08.026.

Buzon, M., Gunter, M., 2017. Current issues with purported "asbestos" content of talc: part 2, examples in hydrothermal hosted talc ores. In: SME Annual Meeting, February 21–24, Phoenix, AZ. https://doi.org/10.19150/trans.8109.

Chidester, A.H., 1962. Petrology and geochemistry of selected talc-bearing ultramafic rocks and adjacent country rocks in North-Central Vermont. Geol. Surv. Prof. Pap. 345.

Chidester, A.H., Engel, A.E., Wright, L.A., 1964. Talc resources of the United States. In: Geological Survey Bulletin 1167. USGS Open-File Report. https://pubs.usgs.gov/bul/1167/report.pdf.

Cralley, L.J., Key, M.M., Groth, D.H., Lainhart, W.S., Ligo, R.M., 1968. Fibrous and mineral content of cosmetic talcum products. Am. Ind. Hyg. Assoc. J. 29, 350–354. https://doi.org/10.1080/00028896809343015.

Cymes, B.A., Krekeler, M.P.S., Nicholson, K.N., Grigsby, J.D., 2017. A transmission electron microscopy (TEM) study of silver nanoparticles associated with mine waste from New Caledonian nickel deposits: potential origins of silver toxicity in a world heritage site. Environ. Earth Sci. 76, 640. https://doi.org/10.1007/s12665-017-6978-x.

Cymes, B.A., Almquist, C., Krekeler, M.P.S., 2020. Europium-doped cryptomelane: multi-pathway synthesis, characterization, and evaluation for the gas phase catalytic oxidation of ethanol. Appl. Catal. A Gen. 589, 117310.

Cymes, B., Almquist, C.A., Krekeler, M.P.S., 2021. Effects of Mn(II) and Eu(III) cation exchange in sepiolite-titanium dioxide nanocomposites in the photocatalytic degradation of Orange G. ChemistrySelect 6, 5180–5190. https://doi.org/10.1002/slct.202100303 doi: 10.1016/j.apcata.2019.117310.

Dietrich, M., Wolfe, A., Burke, M., Krekeler, M.P.S., 2019. The first pollution investigation of road sediment in Gary, Indiana: anthropogenic metals and possible health implications for a socioeconomically disadvantaged area. Environ. Int. 128, 175–192. https://doi.org/10.1016/j.envint.2019.04.042.

El-Sharkawy, M.F., 2000. Talc mineralization of ultramafic affinity in the Eastern Desert of Egypt. Mineral. Deposita 35, 346–363. https://doi.org/10.1007/s001260050246.

Ersoy, B., Dikmen, S., Yildiz, A., Gören, R., Elitok, Ö., 2013. Mineralogical and physicochemical properties of talc from Emirdag, Afyonkarahisar, Turkey. Turk. J. Earth Sci. 22 (4), 8. https://doi.org/10.3906/yer-1112-14.

Flett, L., McLeod, C.L., McCarty, J., Shaulis, B., Fain, J.J., Krekeler, M.P.S., 2021. Providing environmental health contexts for native American populations on the Spokane reservation, WA: insights from tree bark particulate matter surrounding the midnite uranium mine. Environ. Res. 194, 110619 https://doi.org/10.1016/j.envres.2020.110619.

Gatta, G.D., Merlini, M., Valdre, G., Liermann, H., Nenert, G., Rothkirch, A., Kahlenberg, V., Pavese, A., 2013. On the crystal structure and compressional behavior of talc: a mineral of interest in petrology and material science. Phys. Chem. Miner. 40, 145–156. https://doi.org/10.1007/s00269-012-0554-4.

Gil, G., Borowski, M.P., Barnes, J.D., Jokubauskas, P., Bagiński, B., Gunia, P., Ilnicki, S., 2022. Formation of serpentinite-hosted talc in a continental crust setting: petrographic, mineralogical, geochemical, and O, H, and Cl isotopic study of the Giłów deposit, Góry Sowie Massif (SW Poland). Ore Geol. Rev. 146, 104926 https://doi.org/10.1016/j.oregeorev.2022.104926.

Girion, L., 2018. Johnson & Johnson Knew for Decades that Asbestos Lurked in its Baby Powder. Reuters. https://www.reuters.com/investigates/special-report/johnsonandjohnson-cancer/.

Greene, R.C., 1995. Talc resources of the conterminous United States. In: USGS Open-File Report, pp. 95–586. https://pubs.usgs.gov/of/1995/0586/report.pdf.

IARC, 2012. Chromium (VI) Compounds. https://monographs.iarc.fr/wp-content/uploads/2018/06/mono100C-9.pdf.

IARC, 2012b. Nickel and Nickel Compounds. https://monographs.iarc.fr/wp-content/uploads/2018/06/mono100C-10.pdf.

Interagency Working Group on Asbestos in Consumer Products (IWGACP), 2021. White Paper: IWGACP Scientific Opinions on Testing Methods For Asbestos In Cosmetic Products Containing Talc. https://www.fda.gov/food/cfsan-constituent-updates/fda-releases-white-paper-testing-methods-asbestos-cosmetic-products-containing-talc.

IRSST, 2012. The Robert-Suave Research Institute in Occupational Health and Safety ("IRSST"). Studies and Research Projects Synthesis of Knowledge on Tremolite in Talc. http://www.irsst.qc.ca/media/documents/PubIRSST/R-755.pdf.

Joshi, P., Sharma, R., 2015. Fluid inclusion and geochemical signatures of the talc deposits in Kanda area, Kumaun, India: implications for genesis of carbonate hosted talc deposits in Lesser Himalaya. Carbonates Evaporites 30, 153–166. https://doi.org/10.1007/s13146-014-0196-3.

Karlsen, T.A., Rian, E., Olesen, O., 2000. Overview of talc resources and reserves in the Altermak talc province, northern Norway and possible uses of the talc ore. Norges

Geol. Unders. Bull. 436, 93–102. Available online: https://www.ngu.no/upload/Publikasjoner/Bulletin/Bulletin436_93-102.pdf [Accessed July 29, 2023].

Kelley, K.A., Plank, T., Ludden, J., Staudigel, H., 2003. Composition of altered oceanic crust at ODP sites 801 and 1149. Geochem. Geophys. Geosyst. 4 (6) https://doi.org/10.1029/2002GC000435.

Klein, E., Krekeler, M.P.S., 2020. The occurrence of Hg, Se, S, Ni, Cr, and Th in talc ore: a scanning electron microscopy (SEM) study of historical samples from the Willow Creek mine, Montana. Results Geochem. 1, 100003 https://doi.org/10.1016/j.ringeo.2020.100003.

Krekeler, M.P.S., Calkins, K., Borkiewicz, O., 2010. Mineralogical and hydrogeologic properties of a partially unconsolidated Pleistocene limestone in the east Central Yucatán: implications for the development of subsurface flow constructed wetlands in the region. Carbonates Evaporates 25, 77–86. https://doi.org/10.1007/s13146-010-0009-2.

Kuisma-Kursula, P., 2020. Accuracy, precision, and detection limits of SEM–WDS, SEM–EDS and PIXE in the multi-elemental analysis of medieval glass. X-Ray Spectrom. 29, 111–118. https://doi.org/10.1002/(SICI)1097-4539(200001/02)29:1<111::AID-XRS408>3.0.CO;2-W.

Landen, X., 2018. Vermont Talc at Center of $117 Million Contaminated Baby Powder Case. https://vtdigger.org/2018/04/16/vermont-talc-center-117-million-contaminated-baby-powder-case.

Laperche, V., Lemière, B., 2021. Possible pitfalls in the analysis of minerals and loose materials by portable XRF, and how to overcome them. Minerals 11, 33. https://doi.org/10.3390/min11010033.

LeGalley, E., Krekeler, M.P.S., 2013. A mineralogical and geochemical investigation of street sediment near a coal-fired power plant in Hamilton, Ohio: an example of complex pollution and cause for community health concerns. Environ. Pollut. 176, 26–35. https://doi.org/10.1016/j.envpol.2012.12.012.

Lindeman, C., Oglesbee, T., McLeod, C.L., Krekeler, M.P.S., 2020. Mineralogy and geochemistry of the Kinnikinic Quartzite at the Arco Hills Silica and gold project in Butte County, Idaho: results of an ore quality spot check and implications for potential plasma furnace processing. Minerals 10, 523. https://www.mdpi.com/2075-163X/10/6/523/pdf.

Loftus, P., 2020. Johnson & Johnson to Stop Selling Talcum Baby Powder in U.S., Canada. https://www.wsj.com/articles/johnson-johnson-to-stop-selling-talcum-baby-powder-in-u-s-canada-11589922588.

Lüchtrath, H., Schmidt, K.C., 1959. Talc and steatite, their relations with asbestos and their effect in intratracheal animal experiments on rats. Beitr. Silikoseforsch. 61, 160.

Mansur, E.T., Barnes, S.J., Duran, C.J., 2021. An overview of chalcophile element contents of pyrrhotite, pentlandite, chalcopyrite, and pyrite from magmatic Ni-Cu-PGE sulfide deposits. Mineral. Deposita 56, 179–204. https://doi.org/10.1007/s00126-020-01014-3.

Materials Research L3C, 2020. J&J Talc Global Supply Chain Research Brief, p. 11. https://www.bcpp.org/wp-content/uploads/2020/10/JJ-Talc-Research-Brief-final-25aug2020.pdf.

Millette, J.R., 2015. Procedure for the analysis of talc for asbestos. Microscope 63, 11–20.

National Minerals Information Center, 2022. Talc and Pyrophyllite Statistics and Information. USGS. https://www.usgs.gov/centers/national-minerals-information-center/talc-and-pyrophyllite-statistics-and-information.

NBC News, 2019. Johnson & Johnson to Recall Baby Powder After Asbestos Found. https://www.nbcnews.com/health/health-news/johnson-johnson-recall-baby-powder-after-asbestos-found-n1068686.

Nkoumbou, C., Villieras, F., Njopwouo, D., Yonta Ngoune, C., Barres, O., Pelletier, M., Razafitianamaharavo, A., Yvon, J., 2008. Physicochemical properties of talc ore from three deposits of Lamal Pougue area (Yaounde Pan-African Belt, Cameroon), in relation to industrial uses. Appl. Clay Sci. 41, 113–132. https://doi.org/10.1016/j.clay.2007.10.006.

Oglesbee, T., McLeod, C.L., Chappell, C., Vest, J., Sturmer, D., Krekeler, M.P.S., 2020. A mineralogical and geochemical investigation of modern Aeolian sands near Tonopah, Nevada: sources and environmental implications. Catena 194, 104640. https://doi.org/10.1016/j.catena.2020.104640.

O'Shea, M., Krekeler, M.P.S., Vann, D.R., Gieré, R., 2021. Investigation of Pb-contaminated soil and road dust in a polluted area of Philadelphia. Environ. Monit. Assess. 193, 440. https://doi.org/10.1007/s10661-021-09213-9.

Paul, K.C., Silverstein, J., Krekeler, M.P.S., 2017. New insights into rare earth element particulate generated by cigarette lighters: an electron microscopy and materials science investigation of a poorly understood indoor air pollutant and constraints for urban geochemistry. Environ. Earth Sci. 76, 369. https://doi.org/10.1007/s12665-017-6687-5.

Pi-Puig, T., Animas-Torices, D.Y., Solé, J., 2020. Mineralogical and geochemical characterization of talc from two Mexican ore deposits (Oaxaca and Puebla) and nine talc marketed in Mexico: evaluation of its cosmetic uses. Minerals 10, 388. https://doi.org/10.3390/min10050388.

Plumlee, G., Morman, S.A., Ziegler, T.L., 2006. The toxicological geochemistry of earth materials: an overview of processes and the interdisciplinary methods used to understand them. Rev. Mineral. Geochem. 64, 5–57. https://doi.org/10.2138/rmg.2006.64.2.

Rohl, A.N., 1974. Identification and quantitation of asbestos in talc. Environ. Health Perspect. 9, 129–132. https://doi.org/10.1289/ehp.74995.

Rohl, A.N., Langer, A.M., Selikoff, I.J., Tordini, A., Klimentidis, R., Bowes, D.R., Skinner, D.L., 1976. Consumer talcums and powders – mineral and chemical characterization. J. Toxicol. Environ. Health 2, 255–284. https://doi.org/10.1080/15287397609529432.

Rosner, D., Markowitz, G., Chowkwanyun, M., 2019. "Nondetected": the politics of measurement of asbestos in talc, 1971-1976. Am. J. Public Health 109, 969–974. https://doi.org/10.2105/AJPH.2019.305085.

Rottier, B., Kouzmanov, K., Wälle, M., Bendezú, R., Fontboté, L., 2016. Sulfide replacement processes revealed by textural and LA-ICP-MS trace element analyses: example from the early mineralization stages at Cerro de Pasco, Peru. Econ. Geol. 111, 1347–1367. https://doi.org/10.2113/econgeo.111.6.1347.

Schandl, E.S., Sharara, N.A., Gorton, M.P., 1999. The origin of the Ashtan talc deposit in the Hamata Area, Eastern Desert, Egypt: a geochemical and mineralogical study. Can. Mineral. 37, 1211–1227.

Shin, D., Lee, I., 2002. Carbonate-hosted talc deposits in the contact aureole of an igneous intrusion (Hwanggangri mineralized zone, South Korea): geochemistry, phase relationships, and stable isotope studies. Ore Geol. Rev. 22, 17–39. https://doi.org/10.1016/S0169-1368(02)00085-9.

Tahir, M., Imai, A., Takahashi, R., Yano, S., 2018. Ore genesis and geochemical characteristics of carbonate-hosted talc deposits in Nangarhar Province, Afghanistan. Resour. Geol. 68 (4), 352–372. https://doi.org/10.1111/rge.12174.

Tchounwou, P.B., Ydejou, C.G., Patlolla, A.K., Sutton, D.J., 2012. Heavy metal toxicity and the environment. In: Luch, A. (Ed.), Molecular, Clinical and Environmental Toxicology. Experientia Supplementum, p. 101. https://doi.org/10.1007/978-3-7643-8340-4_6.

Teklay, A., 2016. Physiological effect of chromium exposure: a review. Int. J. Food Sci. Nutr. Diet. S7, 1–11. https://doi.org/10.19070/2326-3350-SI07001.

Tran, T.H., Steffen, J.E., Clancy, K.M., Bird, T., Egilmana, D.S., 2019. Talc, asbestos, and epidemiology: corporate influence and scientific incognizance. Epidemiology 30, 783–788. https://doi.org/10.1097/EDE.0000000000001091.

Van Gosen, B.S., Berg, R.B., Hammarstrom, J.M., 1998. Map showing areas with potential for talc deposits in the Gravelly, Greenhorn, and Ruby ranges and the Henrys Lake Mountains of southwestern Montana. In: U.S. Geological Survey Open-File Report 98-224-B. https://doi.org/10.3133/ofr98224B.

Van Gosen, B.S., Lowers, H.A., Sutley, S.J., Gent, C.A., 2004. Using the geologic setting of talc deposits as an indicator of amphibole asbestos content. Environ. Geol. 45, 920–939. https://doi.org/10.1007/s00254-003-0955-2.

Velázquez Santana, L.C., McLeod, C.L., Blakemore, D., Shaulis, B., Hill, T., 2020. Bolivian hornblendite cumulates: insights into the depths of Central Andean Arc magmatic systems. Lithos 370-371, 105618. https://doi.org/10.1016/j.lithos.2020.105618.

Vermont Business Magazine, 2018. Talc from Vermont Costs Johnson & Johnso $117 Million in Mesothelioma Case. https://vermontbiz.com/news/2018/april/13/talc-vermont-costs-johnson-johnson-117-million-mesothelioma-case.